Published in final edited form as:
J Phys Chem Lett. 2012 July 19; 3(14): 1858–1864. doi:10.1021/jz3006223.

Fast Detection Allows Analysis of the Electronic Structure of Metalloprotein by X-ray Emission Spectroscopy at Room Temperature

Katherine M. Davis, **Brian A. Mattern**[1], **Joseph I. Pacold**[1], **Taisiya Zakharova**, **Dale Brewe**[2], **Irina Kosheleva**[3], **Robert W. Henning**[3], **Timothy J. Graber**[3], **Steve M. Heald**[2], **Gerald T. Seidler**[1], and **Yulia Pushkar***

Department of Physics, Purdue University, West Lafayette, IN 47907, USA

[1]Department of Physics, University of Washington, Seattle, WA 98195, USA

[2]Advanced Photon Source, Argonne National Laboratory, Argonne, IL 60439

[3]Center for Advanced Radiation Sources, The University of Chicago, Chicago, IL 60637, USA

Abstract

The paradigm of “detection-before-destruction” was tested for a metalloprotein complex exposed at room temperature to the high x-ray flux typical of third generation synchrotron sources. Following the progression of the x-ray induced damage by Mn Kβ x-ray emission spectroscopy, we demonstrated the feasibility of collecting room temperature data on the electronic structure of native Photosystem II, a trans-membrane metalloprotein complex containing a Mn_4Ca cluster. The determined non-damaging observation timeframe (about 100 milliseconds using continuous monochromatic beam, deposited dose $1*10^7$ photons/μm^2 or $1.3*10^4$ Gy, and 66 microseconds in pulsed mode using pink beam, deposited dose $4*10^7$ photons/μm^2 or $4.2*10^4$ Gy) is sufficient for the analysis of this protein’s electron dynamics and catalytic mechanism at room temperature. Reported time frames are expected to be representative for other metalloproteins. The described instrumentation, based on the short working distance dispersive spectrometer, and experimental methodology is broadly applicable to time-resolved x-ray emission analysis at synchrotron and x-ray free-electron laser light sources.

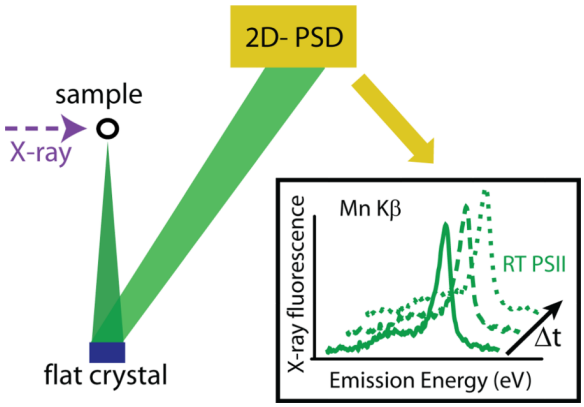

*ypushkar@purdue.edu.

Supporting Information. Spectrometer, sample and experimental details, Figures S1–S6. This material is available free of charge via the Internet at http://pubs.acs.org.

Keywords

X-ray emission spectroscopy (XES); Photosystem II; time-resolved; X-ray induced damage; manganese

Recently developed third generation synchrotron sources and free electron lasers provide unparalleled bright x-ray beams with defined time structure.[1,2] These are indispensible tools for time-resolved structural and functional analysis in chemistry and biology (via crystallography,[3] x-ray scattering[4] and x-ray spectroscopy[5, 6]) as well as for cell and tissue imaging[7]. The main limitation in the application of these x-ray sources and techniques is x-ray induced damage to the materials or biological molecules that can affect their structure and chemical composition.[8, 9] This includes changes in the redox states of metal co-factors and their coordination environment which are thought to occur particularly quickly.[10, 11] One possible way to counteract this damage is to cool biological samples to cryogenic (preferably 10–20K) temperatures.[12] However, this currently routine approach prevents the analysis of dynamics such as electron transfer, conformational changes, and bond formations that occur in biological samples at room temperature (RT). In recent years, and in particular with LCLS coming on-line, it was proposed that the collection of data with sufficiently high time resolution would overcome x-ray damage.[13] The concept for sensitive biological samples is that utilizing setups with high time resolution, we can always define some time window for data collection before x-ray induced damage occurs. While plausible from both a physical and chemical standpoint, it needs experimental validation: in particular, when a biological sample is exposed to the high (full) flux achievable with third generation synchrotron sources.

We chose Photosystem II (PS II) as our biological system due to its high sensitivity to x-ray induced damage.[10, 14, 15] PS II is a central constituent for the natural photosynthetic process that allows for dioxygen formation during photosynthesis occurring in plants, green algae and cyanobacteria. The process of splitting water ($2H_2O \rightarrow O_2 + 4e^- + 4H^+$) in the trans-membrane protein complex of PS II requires a catalyst - the Mn_4Ca cluster, embedded in the unique protein environment. This assembly is termed the oxygen-evolving complex (OEC).[8, 12, 16] There is a substantial scientific interest in uncovering the mechanism of this water splitting catalysis that occurs at room temperature and follows the Kok cycle.[17] This cycle describes five visible light-induced transitions between the so-called S-states (S_0–S_4) corresponding to five redox states of the OEC. In this cycle, oxygen evolves in the $S_3 \rightarrow S_0$ transition and the S_4 state was proposed to represent a transient intermediate.[18, 19]

The mechanism of PS II action can be studied by Mn Kβ x-ray emission spectroscopy (XES) (also known as photon-in-photon-out spectroscopy), Figure 1A, which is highly sensitive to the oxidation state of the Mn centers and spin state of the Mn_4Ca cluster.[20–23] This technique was used here to demonstrate the feasibility of RT XES analysis of the native protein prior to the onset of x-ray induced damage. The Mn Kβ spectra of PS II in several S-states were reported in 2001 from cryogenic (20K) measurements utilizing an x-ray emission spectrometer designed with spherically bent crystal analyzers (SBCA's).[24] Conventional SBCA based setups record emission spectra point-by-point (unless the SBCA is positioned off-Rowland circle)[25] and mechanical movement of the spectrometer/detector assembly is needed to record the next point in the spectrum. This makes such a setup particularly impractical for time-resolved analysis. While cryogenic XES analysis of PS II was available in 2001,[24] no transition of this approach to RT has been reported so far, illustrating associated experimental challenges. To the best of our knowledge, no other metalloprotein has been characterized to date by XES at RT.

To achieve maximal time resolution, we chose to record x-ray emission spectra using dispersive optics that allow for instantaneous detection (Fig. 1B).[26–29] In this implementation, the time resolution of the spectrometer is determined by the time structure of the x-ray beam (x-ray pulses of about 100ps at third generation synchrotron sources, and femtosecond pulses at free electron laser sources). The crystal type and geometry of the spectrometer determine the energy range and resolution, Figures 1, S1–S3.[26–29] While a number of spectrometer designs have been reported previously, no time-resolved experiments have been realized with such a spectrometer, and no feasibility analysis for measurements with dilute / biological samples (in this case, PS II samples have a 0.5mM concentration of Mn ions) has been reported.

This study reports two different miniature x-ray emission spectrometer (miniXES) configurations suitable for the analysis of Mn Kβ emission. The spectrometers use flat dispersive optics and their design is based on the observation that a micro-focused incident beam permits one to obtain good energy resolution from an analyzer crystal located a few centimeters from the sample.[26–29] The first instrument uses the Ge 440 reflection in a Johansson arrangement[30] and allows for a 100 eV collection range containing the Kβ', $K\beta_{1,3}$ (emission from the 3p level) and Kβ'' peaks and demonstrates an instrumental energy resolution of ~1.5 eV, Figures 1D, S2, S3. This instrument allows sufficient space to fit a microfridge assembly into the sample position allowing for low temperature measurements (see SI Materials and Methods and Figure 3B). To improve the energy resolution, the second design instead uses the GaP 440 reflection in a von Hamos configuration[31] Figure S1. This von Hamos design has a decreased collection range of 50 eV, including only the Kβ main lines. However, it demonstrates a higher energy resolution of ~0.3 eV, Figure 1C, D, S1, S3, which is comparable to that of spectrometers utilizing spherically bent crystal analyzers, the instruments heretofore employed for the analysis of PS II.[24] Good energy resolution is evident in the well resolved shoulder on the left side of the MnO $K\beta_{1,3}$, peak as previously observed using traditional instruments, Figure 1D.[20] The majority of room temperature data were collected using the von Hamos spectrometer, Figures 2, 3.

RT XES measurements on the dark-adapted S_1 state of PS II (see SI Material and Methods) were first carried out using monochromatic x-ray beam, see Table 1 for experimental details. During the measurements, a fresh portion of PS II (protected by a synchronized shutter) was exposed to a full intensity monochromatic micro-focused x-ray beam. In order to resolve the onset of x-ray induced damage in time, the acquired images were read from the position sensitive detector (PSD) in defined time intervals: the shortest at ~20 ms. The time required for data read out from the Pilatus detector used in this study is ~ 3ms. Images corresponding to defined exposure times collected from multiple points on the sample were added together. Spectra from different samples were added together after the energy calibration. The summation of PSD images was carried out either in software, when images from single point exposures were collected and stored individually, or by using the spinning sample holder that allowed for simultaneous detection/addition of data from multiple points on the sample, Figure 2B. No differences were observed in spectral shape or time of damage progression between these two methods of data averaging. In Figure 2A, we plot the spectrum obtained in the time interval less than the damage threshold (determined to be 60–100ms while using monochromatic beam, corresponding to $1.3*10^4$ Gy).

Additionally, RT measurements were done with pulsed, pink beam (BioCARS, Advanced Photon Source),[32] Figure 2A and Table 1. Detector images from points on the sample exposed to one, two or more consecutive 22 μsec x-ray pulses were collected and added up. Spectra from different samples were added together after calibration. In Figure 2A, we plot the spectrum obtained using three consecutive x-ray pulses (corresponding to a dose of $4.2.0*10^4$ Gy) that did not show indications of damage.

The time-resolved nature of the XES experiment allowed us to record emission spectra of undamaged PS II at RT and analyze the dose dependent progression of x-ray induced damage (see below). This analysis ensured that data for undamaged PS II were obtained, thus, detection with higher (such as ns or ps) time resolution, technically possible with the described setup, was not necessary for this particular experiment.

To additionally verify that undamaged data were indeed recorded, we used several approaches. 1) Data were visually compared to previously published cryogenic S_1 PS II spectra[24] and found to be identical in terms of spectral shape. Unfortunately, we could not compare the first moment of our PS II spectrum to that reported previously for the S_1 state as no data were provided for a reference compound. 2) We recorded PS II, S_1-state XES at 80K using the Johansson spectrometer design (Figure S2) that allows sufficient space to fit a microfridge assembly into the sample position (see SI Materials and Methods). Obtained RT data were comparable with those taken at 80K. The value of the first moment for RT PS II S_1-state XES agreed well with the value obtained for low temperature spectrum recorded with the same spectrometer, Figure 3. Overall, the x-ray emission spectral shape obtained at RT and low T are similar indicating that no significant charge redistribution is happening within the OEC upon PS II freezing. 3) We did additional analysis of RT Mn K-edge XANES, Figure S4, with equivalent x-ray exposure. Many other studies have documented XANES of the S_1 state and the subsequent x-ray induced damage making it an ideal test to validate our RT damage threshold.[14, 16, 33] Rough XANES scans were taken over short timescales (~23s scans - equivalent to a 4.5 ms exposure at the intensity used for emission measurements with monochromatic x-ray beam) with a seven times reduced incident flux to observe the main edge shift. No shifts were detected with exposures equivalent to 100 ms of the full flux utilized in the XES experiment.

After confirming the time window for the collection of undamaged data, we proceed to analyze the time course of x-ray induced damage. The sensitivity of the $K\beta_{1,3}$ line position to the Mn redox state is used to monitor the photoreduction of the S_1 state (containing two Mn^{III} and two Mn^{IV} ions) resulting in the formation of Mn^{II}.[14, 16, 33] The accumulation of Mn^{II} ions is reflected in a shift to higher energies in the x-ray emission spectra. In the Kβ emission spectrum, the splitting of the Kβ' and $K\beta_{1,3}$ lines is due to the exchange interaction between the 3p hole and the valence electrons on the Mn 3d level. Thus, this splitting is sensitive to the oxidation state of Mn.[20, 32] With the decrease in oxidation state from $Mn^{IV,III}$ to Mn^{II}, the $K\beta_{1,3}$ peak shifts towards higher energies as the number of unpaired electrons increases on the 3d level resulting in larger splitting of the Kβ' and $K\beta_{1,3}$ lines, Figures 2B, 2C.[12, 20, 24, 32] Increases in the Mn^{II} concentration as a function of x-ray exposure were determined by comparing the experimental spectra with calibration spectra. Calibration spectra contained different ratios of Mn^{II} in solution to undamaged S_1 state data. Note that the addition of 10% of Mn^{II} into undamaged data results in a very small shift, thus error bars are included in Figure 3. Typically, for damage analysis ~60– 100ms (RT) and ~60s (low temperature - LT) worth of 2D-PSD exposures were averaged together to improve S/N. Assuming a linear response of the peak shift to the content of Mn^{II} in the sample over small timescales (~ms), then, as a first approximation, we can argue that the damage observed in an averaged set of exposures (100ms for RT and 60s at 80K) actually reflects the damage caused by half the dose deposited during that time frame plus the dose deposited in the time interval/s preceding. Note that we do not assume this linearity across the entire damage profile, only in 'short' averaged exposures. This approximation therefore is much less accurate for the LT data due to the longer exposure times, and causes some shape distortion of the damage profile. The main purpose however, is to accurately depict the dosages over which the damage occurs. Without applying this approximation, the damage threshold would be skewed towards much higher dosages. The ±10% error bars account for the possible uncertainty resulting from a visual comparison of the experimental and

calibration spectra, particularly when comparing data having different energy resolution and therefore different spectral shape (note that 80K measurements were possible only with Ge440 spectrometer - Johansson spectrometer design). The dose dependence of Mn^{II} content (80K) obtained here is similar to that previously reported by the analysis of Mn XANES at 80K, Figure S6.[14]

Figure 3 clearly demonstrates the dramatic increase in the rate of x-ray damage at RT. Previously, the progression of x-ray induced damage to PS II at RT was accessed by Mn K-edge XANES.[15, 34–36] The dependence of damage on the photon dose obtained here is similar to that previously reported, Figure S5. However, one must distinguish these two analyses (XANES and XES) by their different rate of dose deposition. XANES analysis used a flux of $1–5*10^{12}$ photons/s/mm^2 [15, 18] as compared to $1.1*10^{14}$ photons/s/mm^2 of monochromatic beam in this XES study. The comparison indicates that even with a considerably increased (20 times) rate of dose deposition, the damage remains proportional to the accumulated dose and does not display a dependence on the rate of dose deposition. In Grabolle et al.,[15] the lag phase (about 10 sec with $1*10^{12}$ photons/s/mm^2 flux resulting in $1*10^{13}$ photons/mm^2 total exposure) was reported to precede the onset of x-ray damage. This exposure converted to units of μm^{-2} corresponds to $1*10^7$ photons/μm^2, which is comparable to the flux deposited during first 80 ms of our XES experiment with monochromatic beam, Table 1. As we could not visualize any damage in 60– 100 ms exposure time our results do not contradict earlier observations of a lag phase. To further probe the effect of dose deposition rate on the progression of x-ray induced damage to the metal center in the protein, we performed measurements with a pink x-ray beam of high intensity, delivered to the sample in the form of 22 μs pulses. In doing so, we increased the rate of dose deposition approximately 3000 times. We have not observed an increase in the rate of x-ray induced damage under these conditions. Rather, some decrease in the damage was noted, Figure 2C. The statistics of the data set obtained with pink beam were not sufficient for a detailed analysis of damage progression. With a maximum of 20 pulses, we did not achieve full protein damage. This experiment will be repeated in the future for further investigation of damage progression under these conditions.

The obtained damage threshold for RT x-ray studies of PS II confirms that x-ray induced damage will not prevent reliable RT analysis of the S-states of the Kok cycle. This includes the proposed S_4 state (lifetime of a few ms) and its associate electron transfer and bond formation dynamics. We expect other metalloproteins to be similar[11] or less sensitive to x-ray induced damage and, thus, our technical demonstration opens the area of RT XES analysis of metalloproteins with synchrotron sources. In addition, serial femtosecond crystallography, which is currently under development at free electron lasers,[8, 13, 37, 38] can be augmented with the described XES setup to monitor the redox state on metal cofactors in the condition of crystallographic experiments. The present experimental methodology is readily modified to conduct time-resolved analysis of other metalloproteins and to perform laser pump/x-ray probe experiments on proteins, diluted molecular or solid state systems. Its simplicity should allow for a broad adaptation, and its time resolution is only limited by the time structure of the x-ray source.

Experimental Methods

PS II-enriched thylakoid-membrane particles were prepared from spinach.[39, 40] The oxygen evolution 300 μmol O_2/(mg Chl • hr) was measured by a Clark-type electrode. Sample preparation, handling and storage environments were completely dark, save for dim green light. Samples were maintained on ice during preparation.

XES spectra were collected at the Advanced Photon Source (APS) at Argonne National Laboratory on beamlines 20-ID and BioCARS.[32] A Si(111) monochromator was used to prepare the monochromatic beam (Table 1), which was focused using Rh coated KB mirrors. A He filled ion chamber was used to monitor the intensity of the x-rays, I_0. The monochromator was calibrated via the $KMnO_4$ pre-edge, and MnO XES and Fe foil XANES were taken periodically to correct for any shift in energy calibration. The pulsed pink-beam was focused using a KB mirror system with the beam reflecting off the Si stripe to reject higher undulator harmonics. We typically refer to the x-ray beam after passing through the KB mirror system as a "pink beam" since only the low-energy component, below the mirror cutoff, is reflected, see SI. A high-heat-load white-beam x-ray chopper was used to produce a pulse train composed of 22-ms-long x-ray pulses at a rate of 41.1 Hz. This configuration was used for the radiation damage studies. A Si(111) channel-cut monochromator was periodically inserted into the pulsed pink beam ~0.5 m upstream of the fluorescence spectrometer (described below) to enhance the energy resolution for calibration purposes. XES were recorded using a Pilatus (Dectris) 2-dimensional position sensitive detector (2D-PSD).

The two miniature XES spectrometer (miniXES) configurations used have very different characteristics. The first instrument uses the Ge 440 reflection in a Johansson arrangement,[13, 29] and allows for a 100eV collection range containing the Kβ', $K\beta_{1,3}$ and Kβ'' peaks and demonstrates an instrumental energy resolution of ~1.5eV, Figures 1D, S2, S3. The second instrument used the GaP 440 reflection in a von Hamos configuration,[28, 31] Figure S1. This von Hamos design has a decreased collection range of 50eV, including only the Kβ main lines and higher energy resolution of ~0.3eV Figures 1C, 1D, S3.[24] The Mn Kβ spectra obtained for various Mn oxides corresponding to the different oxidation states of Mn were in agreement with previously published results[20, 24] and are not shown here.

An *in situ* calibration of the detector pixels is achieved by measuring the positions of the elastic scattering peaks while scanning the monochromator through the desired x-ray emission energy range, Figure S3. This is done after the completion of the emission measurements. The calibration methodology has been described in detail elsewhere.[26, 28, 29] The 2D-PSD exposures were equivalent to either 7 or 20ms irradiation per sample point. Approximately 25 images were taken per point resulting in a 0.5sec total exposure. To resolve the damage in time, we typically added together ~60–100ms (RT), ~60s (LT) and 3 pulses worth of 2D-PSD exposures to improve S/N, see Figures 2, 3, S5, S6.

Supplementary Material

Refer to Web version on PubMed Central for supplementary material.

Acknowledgments

The research at Purdue was supported by the DOE, Office of Basic Energy Sciences DEFG02- 10ER16184 (YP) and the NSF Graduate Research Fellowship under Grant No. 0833366 (KD). Research at the University of Washington is supported by the DOE, Office of Basic Energy Sciences DE-SC0002194. PNC/XSD facilities at the Advanced Photon Source, and research at these facilities, are supported by the US Department of Energy - Basic Energy Sciences, a Major Resources Support grant from NSERC, the University of Washington, Simon Fraser University and the Advanced Photon Source. Use of the Advanced Photon Source, an Office of Science User Facility operated for the U.S. Department of Energy (DOE) Office of Science by Argonne National Laboratory, was supported by the U.S. DOE under Contract No. DE-AC02-06CH11357. Use of the BioCARS was supported by the National Institutes of Health, National Center for Research Resources, under grant number RR007707. Time-resolved set-up at BioCARS was funded in part through a collaboration with Philip Anfinrud (NIH/NIDDK).

ABBREVIATIONS

OEC	Oxygen evolving complex
XES	x-ray emission spectroscopy
2D-PSD	2-dimensional position sensitive detector
RT	room temperature
LT	low temperature LT
PS II	photosystem II
XANES	x-ray absorption near-edge structure

REFERENCES

1. Young L, et al. Femtosecond Electronic Response of Atoms to Ultra-Intense X-Rays. Nature. 2010; 466(7302):56-U66. [PubMed: 20596013]
2. Bilderback DH, Elleaume P, Weckert E. Review of Third and Next Generation Synchrotron Light Sources. J. Phys. B-At. Mol. Opt. 2005; 38(9):S773–S797.
3. Coppens P. Molecular Excited-State Structure by Time-Resolved Pump-Probe X-Ray Diffraction. What Is New and What Are the Prospects for Further Progress? J. Phys. Chem. Lett. 2011; 2(6): 616–621.
4. Kim J, Kim KH, Kim JG, Kim TW, Kim Y, Ihee H. Anisotropic Picosecond X-Ray Solution Scattering from Photoselectively Aligned Protein Molecules. J. Phys. Chem. Lett. 2011; 2(5):350–356. [PubMed: 21643489]
5. Zhang XY, Smolentsev G, Guo JC, Attenkofer K, Kurtz C, Jennings G, Lockard JV, Stickrath AB, Chen LX. Visualizing Interfacial Charge Transfer in Ru-Dye- Sensitized TiO_2 Nanoparticles Using X-Ray Transient Absorption Spectroscopy. J. Phys. Chem. Lett. 2011; 2(6):628–632.
6. Aziz EF. X-Ray Spectroscopies Revealing the Structure and Dynamics of Metalloprotein Active Centers. J. Phys. Chem. Lett. 2011; 2(4):320–326.
7. Kemner KM, et al. Elemental and Redox Analysis of Single Bacterial Cells by X-Ray Microbeam Analysis. Science. 2004; 306(5696):686–687. [PubMed: 15499017]
8. Lomb L, et al. Radiation Damage in Protein Serial Femtosecond Crystallography Using an X-Ray Free-Electron Laser. Phys. Rev. B. 2011; 84(21) 214111: 1-6.
9. Kuepper K, et al. Magnetic Ground-State and Systematic X-Ray Photoreduction Studies of an Iron-Based Star-Shaped Complex. J. Phys. Chem. Lett. 2011; 2(13):1491–1496.
10. Pushkar Y, Yano J, Sauer K, Boussac A, Yachandra VK. Structural Changes in the Mn_4Ca Cluster and the Mechanism of Photosynthetic Water Splitting. P. Natl. Acad. Sci. USA. 2008; 105(N 6): 1879–1884.
11. Hersleth HP, Andersson KK. How Different Oxidation States of Crystalline Myoglobin Are Influenced by X-Rays. BBA-Proteins Proteom. 2011; 1814(6):785–796.
12. Umena Y, Kawakami K, Shen JR, Kamiya N. Crystal Structure of Oxygen- Evolving Photosystem II at a Resolution of 1.9 Angstrom. Nature. 2011; 473(7345):55-U65. [PubMed: 21499260]
13. Chapman HN, et al. Femtosecond X-Ray Protein Nanocrystallography. Nature. 2011; 470(7332): 73-U81. [PubMed: 21293373]
14. Yano J, et al. X-Ray Damage to the Mn_4Ca Complex in Photosystem II Crystals: A Case Study for Metallo-Protein X-Ray Crystallography. P. Natl. Acad. Sci. USA. 2005; 102:12047–12052.
15. Grabolle M, Haumann M, Muller C, Liebisch P, Dau H. Rapid Loss of Structural Motifs in the Manganese Complex of Oxygenic Photosynthesis by X-Ray Irradiation at 10-300 K. J. Biol. Chem. 2006; 281(8):4580–4588. [PubMed: 16352605]
16. Yano J, Yachandra VK. Where Water Is Oxidized to Dioxygen: Structure of the Photosynthetic Mn_4Ca Cluster from X-Ray Spectroscopy. Inorg. Chem. 2008; 47(6):1711–1726. [PubMed: 18330965]

17. Kok B, Forbush B, McGloin M. Cooperation of Charges in Photosynthetic O_2 Evolution. Photochem. Photobiol. 1970; 11:457–476. [PubMed: 5456273]
18. Haumann M, Liebisch P, Muller C, Barra M, Grabolle M, Dau H. Photosynthetic O-2 Formation Tracked by Time-Resolved X-Ray Experiments. Science. 2005; 310(5750):1019–1021. [PubMed: 16284178]
19. Dau H, Haumann M. Time-Resolved X-Ray Spectroscopy Leads to an Extension of the Classical S-State Cycle Model of Photosynthetic Oxygen Evolution. Photosynth. Res. 2007; 92(3):327–343. [PubMed: 17333506]
20. Glatzel P, Bergmann U. High Resolution 1s Core Hole X-Ray Spectroscopy in 3d Transition Metal Complexes - Electronic and Structural Information. Coord. Chem. Rev. 2005; 249(1–2):65–95.
21. Sauer K, Yano J, Yachandra VK. X-Ray Spectroscopy of the Photosynthetic Oxygen-Evolving Complex. Coord. Chem. Rev. 2008; 252(3–4):318–335. [PubMed: 19190720]
22. Vanko G, Glatzel P, Pham VT, Abela R, Grolimund D, Borca CN, Johnson SL, Milne CJ, Bressler C. Picosecond Time-Resolved X-Ray Emission Spectroscopy: Ultrafast Spin-State Determination in an Iron Complex. Angew. Chem.-Int. Edit. 2010; 49(34):5910–5912.
23. Beckwith MA, Roemelt M, Collomb MN, DuBoc C, Weng TC, Bergmann U, Glatzel P, Neese F, DeBeer S. Manganese K Beta X-Ray Emission Spectroscopy as a Probe of Metal-Ligand Interactions. Inorg. Chem. 2011; 50(17):8397–8409. [PubMed: 21805960]
24. Messinger J, et al. Absence of Mn-Centered Oxidation in the S_2 to S_3 Transition:Implications for the Mechanism of Photosynthetic Water Oxidation. J. Am. Chem. Soc. 2001; 123:7804–7820. [PubMed: 11493054]
25. Huotari S, Albergamo F, Vanko G, Verbeni R, Monaco G. Resonant Inelastic Hard X-Ray Scattering with Diced Analyzer Crystals and Position-Sensitive Detectors. Rev. Sci. Instrum. 2006; 77(5) 053102: 1-6.
26. Dickinson B, Seidler GT, Webb ZW, Bradley JA, Nagle KP, Heald SM, Gordon RA, Chou IM. A Short Working Distance Multiple Crystal X-Ray Spectrometer. Rev. Sci. Instrum. 2008; 79(12) 123112:1-8.
27. Seidler, G. Patent Application Us 2011/0058652 A1 Short Working Distance Spectrometer and Associated Devices, Systems and Methods 2010.
28. Mattern BA, Seidler GT, Haave M, Pacold JI, Gordon RA, Planillo J, Quintana J, Rusthoven B. A Plastic Miniature X-Ray Emission Spectrometer (MiniXES) Based on the Cylindrical Von Hamos Geometry. Rev. Sci. Instrum. 2012; 83 023901: 1-9.
29. Pacold JI, et al. A Miniature X-Ray Emission Spectrometer (MiniXES) for High- Pressure Studies in a Diamond Anvil Cell. J. Synchrotron Radiat. 2012; 19:245–251. [PubMed: 22338686]
30. Johansson T. A Novel, Accurate-Focusing X-Ray Spectrometer. Zeitschrift Fur Physik. 1933; 82(7–8):507–528.
31. von Hamos L. Roetgen Spectra Image by Means of the Crystal Effect. Ann. Phys.-Berlin. 1933; 17(6):716–724.
32. Graber T, et al. Biocars: A Synchrotron Resource for Time-Resolved X-Ray Science. J. Synchrotron Radiat. 2011; 18:658–670. [PubMed: 21685684]
33. Macedo S, Pechlaner M, Schmid W, Weik M, Sato K, Dennison C, Djinovic-Carugo K. Can Soaked-in Scavengers Protect Metalloprotein Active Sites from Reduction During Data Collection? J. Synchrotron Radiat. 2009; 16:191–204. [PubMed: 19240331]
34. Haumann M, Grabolle M, Neisius T, Dau H. The First Room-Temperature X-Ray Absorption Spectra of Higher Oxidation States of the Tetra-Manganese Complex of Photosystem II. FEBS Lett. 2002; 512(1–3):116–120. [PubMed: 11852063]
35. Haumann M, Muller C, Liebisch P, Iuzzolino L, Dittmer J, Grabolle M, Neisius T, Meyer-Klaucke W, Dau H. Structural and Oxidation State Changes of the Photosystem II Manganese Complex in Four Transitions of the Water Oxidation Cycle (S-0 ->S-1, S-1 ->S-2, S-2 ->S-3, and S-3,S-4 ->S-0) Characterized by X-Ray Absorption Spectroscopy at 20 K and Room Temperature. Biochemistry. 2005; 44(6):1894–1908. [PubMed: 15697215]
36. Meinke C, Sole VA, Pospisil P, Dau H. Does the Structure of the Water-Oxidizing Photosystem II-Manganese Complex at Room Temperature Differ from Its Low-Temperature Structure? A

Comparative X-Ray Absorption Study. Biochemistry. 2000; 39(24):7033–7040. [PubMed: 10852700]

37. Hunter MS, Fromme P. Toward Structure Determination Using Membrane-Protein Nanocrystals and Microcrystals. Methods. 2011; 55(4):387–404. [PubMed: 22197730]
38. Boutet S, Williams GJ. The Coherent X-Ray Imaging (CXI) Instrument at the Linac Coherent Light Source (Lcls). New. J. Phys. 2010; 12 023901: 1-25.
39. Rutherford AW. Orientation of Electron-Paramagnetic-Res Signals Arising from Components in Photosystem-II Membranes. Biochim. Biophys. Acta. 1985; 807(2):189–201.
40. Berthold DA, Babcock GT, Yocum CF. A Highly Resolved, Oxygen-Evolving Photosystem-II Preparation from Spinach Thylakoid Membranes - Electron-Paramagnetic-Res and Electron-Transport Properties. FEBS Lett. 1981; 134(2):231–234.

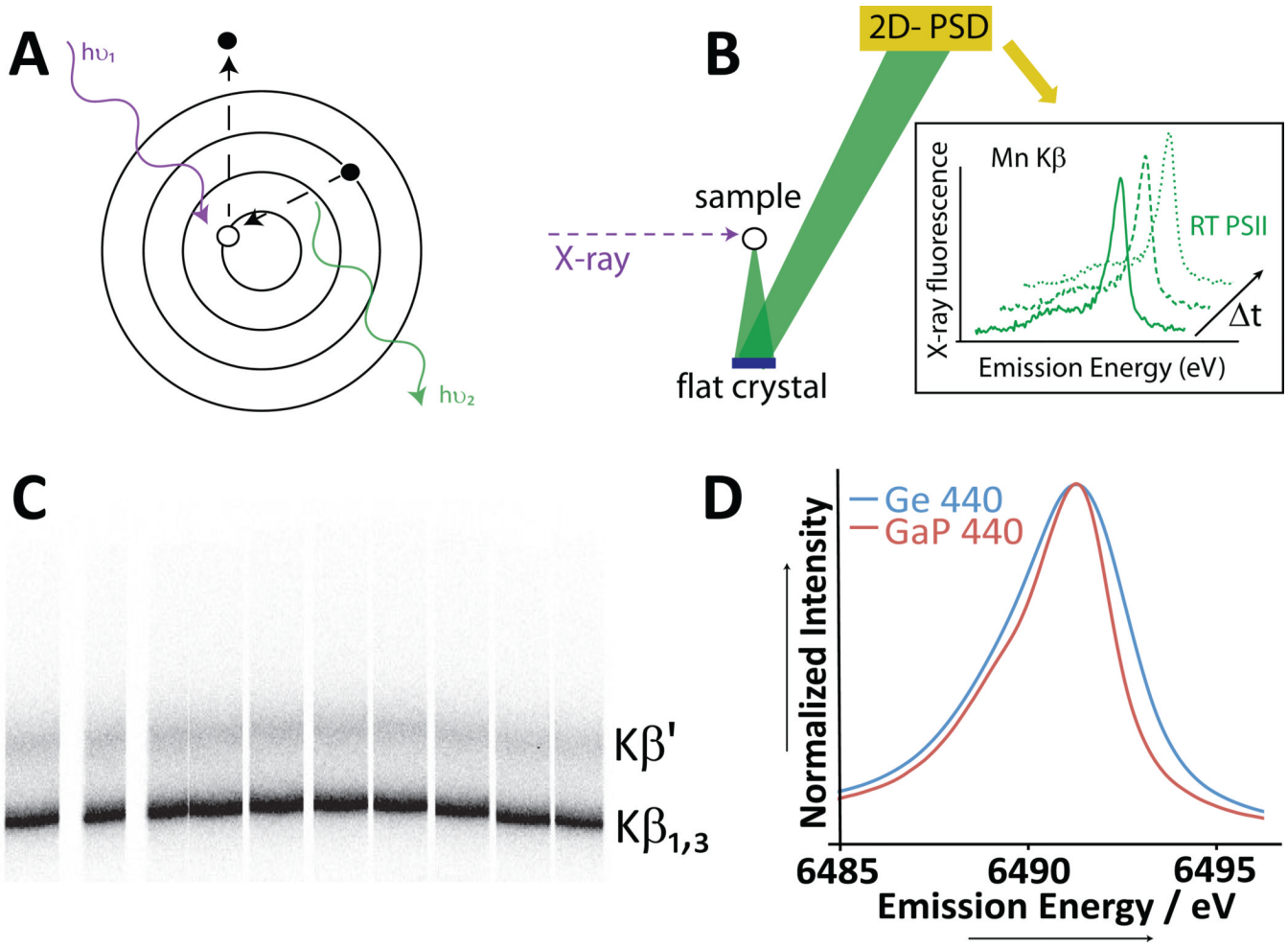

Figure 1.

(A) Absorption of the x-ray photon results in the ejection of a 1s core shell electron and the subsequent repopulation of the created hole with electron from 3p level (Kβ emission lines). (B) Resulting x-ray fluorescence is reflected by a flat crystal onto the position sensitive detector (PSD). Data from the PSD are read out in defined time intervals, Δt. Pixel-to-energy calibration of PSD allows reconstruction of the XES spectrum. (C) Mn Kβ main lines in MnO are recorded on a 2D-PSD. (D) Comparison of MnO Kβ spectra obtained with two reported spectrometers. The GaP 440 von Hamos miniXES demonstrates an energy resolution comparable to that of spectrometers using spherically bent crystal analyzers.[24]

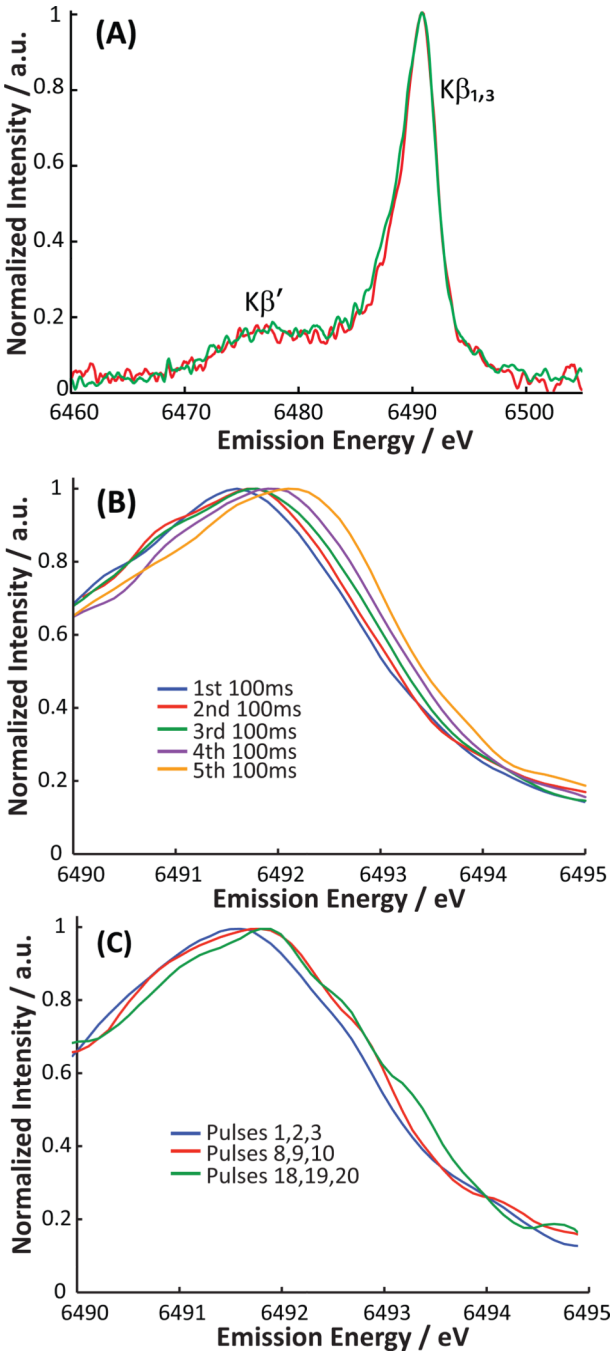

Figure 2.

(A) Mn Kβ x-ray emission spectra for the undamaged OEC of PS II recorded at room temperature using continuous monochromatic (green) and pulsed pink (red) x-ray beams. The total amount of PS II protein used to obtain displayed spectra is ~80 mg (green) and ~40mg (red). Linear background (about 30% (green)/50% (red) of the signal intensity), was subtracted, see Materials and Methods. (B & C) Effect of the progression of x-ray induced damage on the Mn Kβ XES spectra of the PS II obtained using the rotating sample holder. Data are shown for consecutive 100ms exposures with continuous X-ray illumination (B) and in intervals of three pulses of the x-ray beam (C). The shift of the XES spectrum to

higher energy is due to the photoreduction of the OEC containing Mn^{III} and Mn^{IV} ions to Mn^{II}.

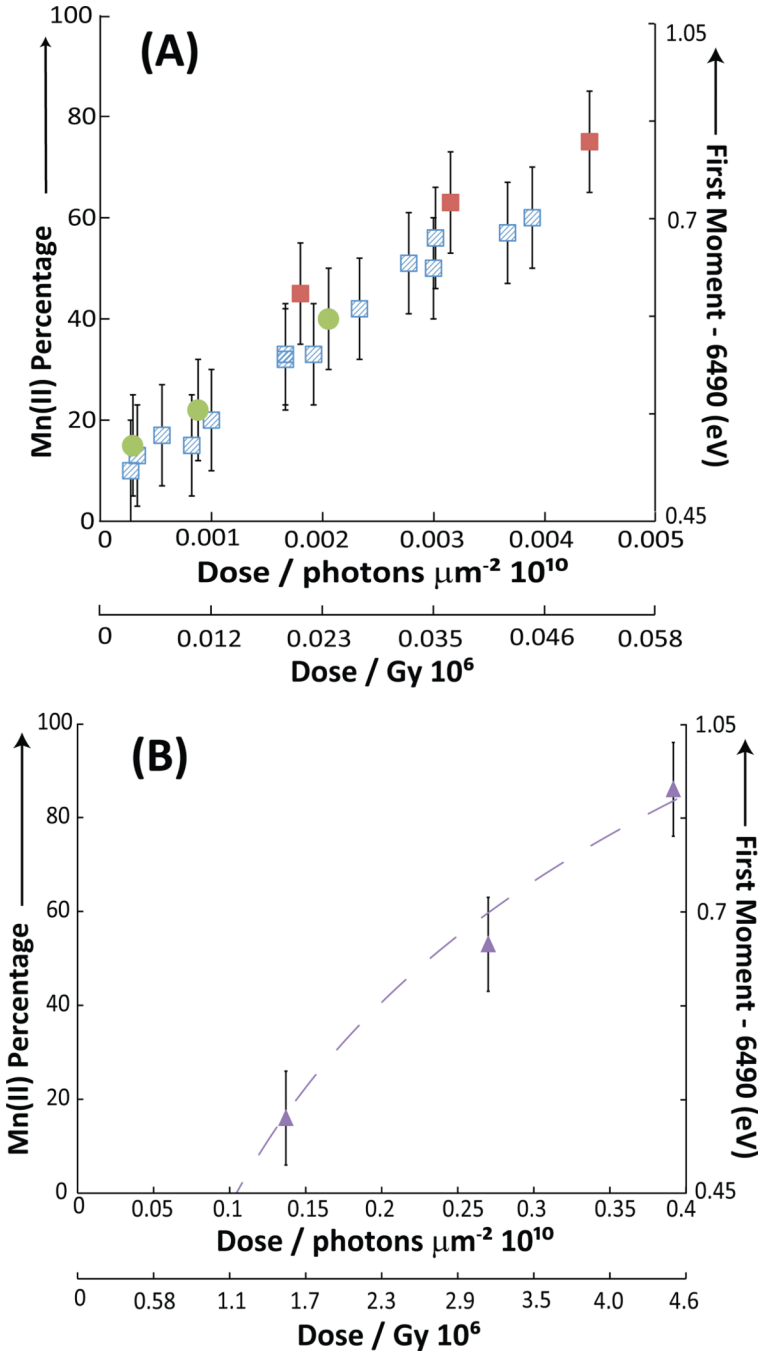

Figure 3.

X-ray induced damage to the OEC expressed as a percentage of Mn^{II} plotted versus photon dose for RT (A) and 80K (B) data, note difference in the x-axis. (A) RT data were collected from the Johansson (red squares, excitation energy 7.5 keV, static sample holder), and von Hamos miniXES (blue striped squares and green circles – corresponding to dynamic and static sample holders, excitation energy 7.09 keV) spectrometers, respectively. (B) The purple triangular data were recorded with the Johansson spectrometer at 80K, and excitation energy of 7.5keV. Energy scales for all data are relative to the MnO reference compound (first moment 6490.82 eV). Also, note that 1^{st} moments are sensitive to procedures of the background removal and noise in the spectra.

Table 1

Comparison of the experimental parameters for continuous beam and pulsed mode.

Experimental Characteristics	20-ID: Monochromatic beam	BioCARS: Pink Beam
Excitation Energy (keV)	7.09 or 7.5 (indicated in the text)	peak energy centered at 7.85keV
Photon Flux	~10^{12} photons per second	~7×10^{10} photons in 22 μs pulse
Spot size on the sample (μm^2 – vert. × horiz.)	~106 × 85	~43 × 120
Shortest exposure	20ms	22 μs
Dose delivered in the shortest exposure, photons/μm^2	$2.2*10^6$	$1.36*10^7$
Dose delivered in the shortest exposure, Gy *	$0.26*10^4$	$1.4*10^4$
Pink beam repetition rate	n/a	41.1Hz

* Dosages in grays were calculated assuming a sample thickness equivalent to one penetration length (distance at which the x-ray intensity is attenuated by a factor of *e*, approximately equal to 2.7 times) at Mn Kβ emission energy (6490 eV). For PS II solution approximated as water, one penetration depth is equal 520μm. For the measurements at BioCARS, the incident energy was assumed to be 7.85keV, while the real incident beam had a spread of energies centered at 7.85keV).